Gravity Disturbances, Marussi Tensor, Invariants and Other Functions of the Geopotential Represented by EGM 2008

J. Klokočník[*1], J. Kostelecký[2], J. Kalvoda[3], L. V. Eppelbaum[4], A. Bezděk[5]

[*1, 5]Astronomical Institute, Academy of Sciences of the Czech Republic, CZ-25165 Ondřejov, Fričova 298, Czech Republic

[2]Research Institute of Geodesy, Topography and Cartography, CZ-25066 Zdiby 98, Czech Republic

[3]Faculty of Science, Charles University in Prague, CZ-12843 Praha 2, Albertov 6, Czech Republic

[4]Dept. of Geophysical, Atmospheric & Planetary Sciences, Tel Aviv University, Ramat Aviv 69978, Tel Aviv, Israel

[1]jklokocn@asu.cas.cz; [2]kost@fsv.cvut.cz; [3]kalvoda@natur.cuni.cz; [4]levap@post.tau.ac.il; [5]bezdek@asu.cas.cz

Abstract-Gravity disturbances, the Marussi tensor, invariants of the gravity field, their certain ratio and other functions of the geopotential (including newly defined "virtual deformations") are computed based on the harmonic coefficients of the global gravitational field model EGM 2008. Regional examples of correlations of large-scale morphotectonic and landform patterns with some aspects of the geopotential as computed from the EGM 2008 are presented. It is suggested that morphotectonic and landform patterns with very conspicuous combinations of significantly high positive or negative values of Γ_{33} are under the strong influence of rapid and/or intensive geomorphic processes. These geophysical signatures supported by values of the strike angle θ_S and virtual dilatations or compressions of the ellipse of deformation reflect the regional dynamics of Earth surface evolution as characterised by very effective integration of tectonic and climate-driven morphogenetic processes.

Keywords- Earth Gravitational Model 2008; Gravity Disturbances; Marussi Tensor; Invariants of the Gravity Field; Virtual Deformations of the Ellipse of Deformation; Landform Patterns; Geodynamics

I. INTRODUCTION AND TOPICS OF THE STUDY

Global combined gravitational field models of the Earth, based on satellite and terrestrial data, can obtain worldwide high resolution today. *The Earth Gravitational Model* 2008 (EGM 2008, see [1-3]) uses multiyear inter-satellite range-rate data from a near polar orbiting tandem of satellites called GRACE (*G*ravity *R*ecovery and *C*limate *E*xperiment, NASA and DLR) via the gravitational model ITG-GRACE03S [4] and extensive gravity anomalies derived from terrestrial or airborne gravimeters and satellite altimetry. GRACE data are the sole data for this model over Antarctica. EGM 2008 reaches a resolution of 5x5 arcmin, which is ~9 km half-wavelength on the Earth's surface at the equator, and, with the exception of Antarctica and some other areas, a precision of the order 1 milliGal (mGal). This is not only claimed by the authors of the model but a result confirmed by extensive tests, see, e.g. [5].

Such a model offers new opportunities to many applications in geodesy, geophysics, geology, geomorphology and physical geography. The new data coming from the gradiometer on board GOCE (*G*ravity Field and Steady-State *O*cean *C*irculation *E*xplorer, ESA's gravity mission, see [6]) have improved the middle-wavelength part (from degree of geopotential harmonics ~120 to ~250). The EGM 2008 lacks adequate precision at higher degrees in some areas, not only in Antarctica, but also in mountain ranges such as the Ands and the Himalaya (more details in Figs. 1 and 2).

In this paper, we compute the following quantities, by using the geopotential coefficients of the EGM 2008: the geoid undulations N [m], the gravity anomalies Δg (or disturbances) [1 mGal = 10^{-5} ms^{-2}], the full Marussi tensor of the second derivatives of the disturbing potential (1E = 1 Eötvös = 10^{-9} s^{-2}), namely its radial component Γ_{33} (sometimes denoted T_{zz} or T_{rr}) in spherical harmonics, the invariants of the gravity field I_0, I_1, I_2, computed from the components of the Marussi tensor, their specific ratio I and the strike angle θ, utilizing the theory of Pedersen and Rasmussen [7] and Beiki and Pedersen [8]. A "virtual deformation" is added; the motivation is to get some ideas about possible dynamic features concealed in the static gravity field data. Some of the quantities mentioned above are functionals of the geopotential in a mathematical sense while some of them are not. Therefore, they are concisely designated in the paper as *"aspects"* of the geopotential.

The second order derivatives and the invariants provide evidence about details of near-surface (not deep) structures. The Marussi tensor was already used locally (areas of a few kilometres) for petroleum, metal, diamond, groundwater etc. explorations (e.g. [9, 10]). The full Marussi tensor is a rich source of information derived from gravity anomalies providing useful details about objects closely locating to the Earth's surface. This extra information can be used by tensor imaging techniques to enhance target anomalies, as tested for local features (economic minerals, oil and gas deposits, fault location, etc.), see, e.g., [10, 11].

Theoretical and experimental studies mentioned above are our stimulation to examine larger regions - in other words, to advance from local gradiometric measurements to the global gravity field models. Previously regional gravity anomalies or the

second derivatives were derived from gravimeters or gradiometers placed on aircrafts. Recently, Beiki and Pedersen [8] tested an approach to the larger area (500 x 500 km) of the Vredefort impact crater in South Africa. These authors also used local measurements (airborne gravity gradiometric data) but not geopotential coefficients.

For the first time, we computed the aspects listed above, based on the global gravity field model. The resolution achieved by the EGM 2008 is applicable and valuable for regional (10^2 – 10^3 km) and large-scale surveys. The local scale (~1 km) is below the resolution of the EGM 2008. Tests of the sensitivity of the aspects of the EGM 2008 to selected landform patterns were realized by Klokočník et al. [12, 13] using large impact craters and by Kalvoda et al. [5, 14] in Himalaya and other regions with conspicuous relief features of active orogeny and intensive climate-morphogenetic processes.

The aim of this paper is to present examples of the aspects computed with the EGM 2008, with suggestions of various geomorphological and geodynamic interpretations. This study is about the methodology and technique of the gravity data processing, not primarily about any interpretation. Computed results are only shortly commented as a motivation for further possible geoapplications by other specialists.

II.   THEORY, DATA AND COMPUTATIONS

The disturbing static gravitational potential outside the Earth masses in spherical coordinates in spherical harmonic expansion is given by the formula:

$$T(r, \varphi, \lambda) = \frac{GM}{r} \sum_{l=2}^{\infty} \sum_{m=0}^{l} \left(\frac{R}{r}\right)^l \left(C'_{l,m} \cos m\lambda + S_{l,m} \sin m\lambda\right) P_{l,m}(\sin \varphi) \tag{1}$$

where *GM* is a product of the universal gravity unit and the mass of the Earth (also known from satellite analyses as a geocentric gravitational constant), *r* is the radial distance of an external point where *T* is computed, *R* is for the radius of the Earth (which can be approximated by the semi-major axis of a reference ellipsoid), $P_{l,m}$ *(sin φ)* are Legendre associated functions, *l* and *m* are the degree and order of the harmonic expansion, (*φ, λ*) are geocentric latitude and longitude, $C'_{l,m}$ and $S_{l,m}$ are harmonic geopotential coefficients (Stokes parameters), fully normalized, $C'_{l,m} = C_{l,m} - C^{el}_{l,m}$, where $C^{el}_{l,m}$ belongs to the reference ellipsoid.

Gravity gradient tensor **Γ** (the Marussi tensor) is a tensor of the second derivatives of the disturbing potential V of the particular gravitational field model known to the maximum degree l_{max} (see below details about EGM 2008). The second derivatives are expressed in the local North-oriented reference frame (*x*, *y*, *z*), where *z* has the geocentric radial direction, *x* points to the north, and *y* is directed to the West [6]:

$$\mathbf{\Gamma} = \begin{bmatrix} \Gamma_{11} & \Gamma_{12} & \Gamma_{13} \\ \Gamma_{21} & \Gamma_{22} & \Gamma_{23} \\ \Gamma_{31} & \Gamma_{32} & \Gamma_{33} \end{bmatrix} = \begin{bmatrix} \frac{\partial^2 V}{\partial x^2} & \frac{\partial^2 V}{\partial x \partial y} & \frac{\partial^2 V}{\partial x \partial z} \\ \frac{\partial^2 V}{\partial y \partial x} & \frac{\partial^2 V}{\partial y^2} & \frac{\partial^2 V}{\partial y \partial z} \\ \frac{\partial^2 V}{\partial z \partial x} & \frac{\partial^2 V}{\partial z \partial y} & \frac{\partial^2 V}{\partial z^2} \end{bmatrix}. \tag{2}$$

The outside of the source masses **Γ** satisfies Laplace's differential equation, the trace of the Marussi tensor is zero, tensor **Γ** is symmetric, and contains just five linearly independent components. These can be conveniently computed by means of the formulae in Hotine [15]. The tensor components (excluding Γ_{33}) are used in local scales to identify and map geological contact information, be it the edges of source targets or structural/stratigraphic contact information. The horizontal components help to identify the shape and geological setting of a target body. The quantity Γ_{33} is best suited for target body detection; Γ_{33} helps to define isopath/density relationships of a body mass with relation to its geological setting, e.g. [10].

Under any coordinate transformation, **Γ** preserves *three invariants*

$$I_0 = trace \ (\mathbf{\Gamma}) = \Gamma_{11} + \Gamma_{22} + \Gamma_{33} \tag{3}$$

$$I_1 = \Gamma_{11}\Gamma_{22} + \Gamma_{22}\Gamma_{33} + \Gamma_{33}\Gamma_{11} - \Gamma_{12}^2 - \Gamma_{23}^2 - \Gamma_{13}^2 \tag{4}$$

$$I_2 = det(\mathbf{\Gamma}) = \Gamma_{11}(\Gamma_{22}\Gamma_{33} - \Gamma_{23}^2) + \Gamma_{12}(\Gamma_{23}\Gamma_{13} - \Gamma_{12}\Gamma_{33}) + \Gamma_{13}(\Gamma_{12}\Gamma_{23} - \Gamma_{13}\Gamma_{22}) \tag{5}$$

Pedersen and Rasmussen [7] showed that the ratio *I* of the I_1 and I_2 defined as

$$0 \le I = -\frac{(I_2/2)^2}{(I_1/3)^3} \le 1 \tag{6}$$

lies between zero and unity for any potential field. If the causative body is strictly 2D, then *I* is equal to zero.

The strike angle θ_S is determined through

$$tan\,2\theta_s = 2\,\frac{\Gamma_{12}(\Gamma_{11} + \Gamma_{22}) + \Gamma_{13}\Gamma_{23}}{\Gamma_{11}^2 - \Gamma_{22}^2 + \Gamma_{13}^2 - \Gamma_{23}^2} = 2\,\frac{-\Gamma_{12}\Gamma_{33} + \Gamma_{13}\Gamma_{23}}{\Gamma_{13}^2 - \Gamma_{23}^2 + \Gamma_{33}(\Gamma_{11} - \Gamma_{22})} \tag{7}$$

within a multiple of $\pi/2$. The strike angle indicates how gradiometer measurements rotate within the main directions of the underground structures. Provided that I is small, the strike angle may indicate a dominant 2-D structure. For more details see [7] or [8].

Pioneer works about satellite gradiometry are [16] about GRADIO or [17] or more generally in Rummel [18, 19], Marussi [20], Hotine [15] and others. The first satellite mission equipped by a gradiometer (differential micro-accelerometer) was GOCE [6]. Methodology and use of the invariants in satellite gradiometry is discussed, e.g., by Baur et al. [21]. In order to find "geometrical meaning" of the invariants and/or to show a deeper relationship of the invariants to the geometry of the gravitational field, Holota [22], see his equations 3.15 - 3.16 and 4.12 - 4.13, derived that the invariants I_1 and I_2 depend on curvatures of the equipotential surface and on the curvature vector of the line of force. For the simplest model of geopotential (gravity point source, monopole) $I_1 = -3\,(GM)^2\,r^{-6}$ and $I_2 = -2\,(GM)^3\,r^{-9}$, indicating a relation to volume of shallow subsurface masses [7]. There are various works about the use of the invariants, see, e.g., [23] or [24].

To define the new term "virtual deformation", we utilize an analogy with the tidal deformation. Similarly as the tidal force shifts and deforms the Earth, an inhomogeneous gravity field of the Earth could act analogically. Subsequently, we can imagine directions of such deformations due to "erosion" brought about "gravity origin". We can also say that the virtual deformations indicate preferred directions of solely gravity transport of the matter of rock massifs at surface of a planet.

If there is tidal potential T, then horizontal shifts (deformations) exist due to it and they can be expressed as follows: in North-South direction (latitude direction)

$$u_\Phi = l_S\,\frac{1}{g}\frac{\partial T}{\partial \varphi} \tag{8}$$

in East-West direction (longitudinal direction)

$$u_\Lambda = l_S\,\frac{1}{g\cos\varphi}\frac{\partial T}{\partial \lambda} \tag{9}$$

where g is gravity acceleration 9.81 m·s^{-2}, l_S is elastic coefficient (Shida number) expressing the elastic properties of the Earth as a whole planet ($l_S = 0.08$), φ and λ are the geocentric coordinates (latitude and longitude) of a point P where we measure T; the potential T in [m^2·s^{-2}]. In our case, T is represented by Eqs. (1), (8) and (9). This mechanism is applied to a standard Earth model (here EGM 2008), but the real values of the Shida parameters l for the Earth's surface (for our task) are not known.

We apply the apparatus of mechanics of continuum to derive the main directions of the tension (e.g., Brdička et al. [25]). The tensor of (small) deformation $\boldsymbol{E}$ is defined as a gradient of shift. Let us select a local coordinate system (x, y) in P by the equations

$$R.\,d\varphi = dx, \quad R.\,d\lambda \cos\varphi = dy,$$

where R is mean radius of the Earth. Then it holds that

$$\boldsymbol{E} = \begin{pmatrix} \epsilon_{11} & \epsilon_{12} \\ \epsilon_{21} & \epsilon_{22} \end{pmatrix} = grad(\mathbf{d}) = \begin{pmatrix} \dfrac{\partial u_x}{\partial x} & \dfrac{\partial u_x}{\partial y} \\ \dfrac{\partial u_y}{\partial x} & \dfrac{\partial u_y}{\partial y} \end{pmatrix} \tag{10}$$

$$\mathbf{d} = \boldsymbol{E}\,\mathbf{x} + \mathbf{t}$$

where $\mathbf{d}$ is the vector of shift, $\boldsymbol{E}$ the gradient of shift, $\mathbf{x}$ the vector of the coordinates and $\mathbf{t}$ is the vector of translation. The tensor of deformation can be separated into two parts:

$$\boldsymbol{E} = \mathbf{e} + \boldsymbol{\Omega} = \big(e_{ij}\big) + \big(\Omega_{ij}\big) \tag{11}$$

where $\mathbf{e}$ is the symmetrical tensor and $\boldsymbol{\Omega}$ the anti-symmetrical tensor of deformation, respectively. The symmetrical tensor is:

$$\mathbf{e} = \begin{pmatrix} e_{11} & e_{12} \\ e_{21} & e_{22} \end{pmatrix} = \begin{pmatrix} \epsilon_{11} & (\epsilon_{12} + \epsilon_{21})/2 \\ (\epsilon_{12} + \epsilon_{21})/2 & \epsilon_{22} \end{pmatrix} \tag{12}$$

and the parameters of deformation are:

$\Delta = e_{11} + e_{22}$ total dilatation

$\gamma_1 = e_{11} - e_{22}$ pure cut

$\gamma_2 = 2e_{12}$ technical cut

$\gamma = (\gamma_1{}^2 + \gamma_2{}^2)^{1/2}$		total cut
$a = \frac{1}{2}(\Delta + \gamma)$		major semi-axis of ellipse of deformation
$b = \frac{1}{2}(\Delta - \gamma)$		minor semi-axis of ellipse of deformation
$\alpha = \frac{1}{2}\operatorname{atan}(\gamma_2 / \gamma_1)$		direction of main axis of deformation.

In relevant sketch maps of the complex figures, which are a substantial part of the 3rd chapter, the semi-axes of deformation ellipse a and b are expressed together with their relative size. Values of l_S are not known, and, therefore, only main directions of the virtual deformations (and not also their amplitudes) are demonstrated. The plotted quantities are a and b expressed in the figures as small crosses.

Virtual deformations of the ellipse of deformation, calculated using the tensor of deformation $\boldsymbol{E}$ (Eqs. (8) - (12)), are geometrically expressed by its dilatation or compression. The virtual dilatation indicates uplifted regions at the geoid, whose mass has (owing or according to the pattern of values of the gravitational potential) a tendency to disintegration. On the contrary, the virtual compression indicates lowered zones and/or areas at the geoid. Natural processes, which are the cause of these states of the near-surface part of the geoid, are certainly very diverse as a consequence of regionally heterogeneous integration of morpho-tectonic and erosion-denudation processes.

The EGM 2008 [1-3] is a combined solution (from satellite and terrestrial data) complete to the degree and order 2160 in a spherical harmonic expansion. It also contains additional coefficients extending to the degree 2190 and order 2159. Satellite data to the EGM 2008 come from the GRACE A/B SST (low-low satellite-to-satellite tracking). The terrestrial data base of EGM2008 is very extensive; it consists of several sources: gravimetric measurements, anomalies derived from altimetry, models or fill-in data from digital models of the terrain relief when nothing better was available (Fig. 1a). EGM 2008 is probably the best currently available combination gravity field model of the Earth. Nevertheless, it does not yield a homogeneous gravity anomaly field. For example, no terrestrial data in the EGM 2008 are available for Antarctica. Only poorer data (the "fill-in" set from satellite topography, of lower precision, resolution and reliability) over high mountain belts and some other areas are available (Pavlis et al. [3]). The regional structure of data sources for the EGM 2008 and related explanations are shown in Fig. 1.

Although the data in EGM 2008 are of high quality in general, there are still large variations of the precision of the geoid undulation, gravity anomalies, and other quantities derived from C_{lm}, S_{lm} of EGM 2008. Fig. 2 documents the accuracy estimates (commission error) for the gravity anomalies in EGM 2008, their variability over latitude and longitude from covariance analysis [1].
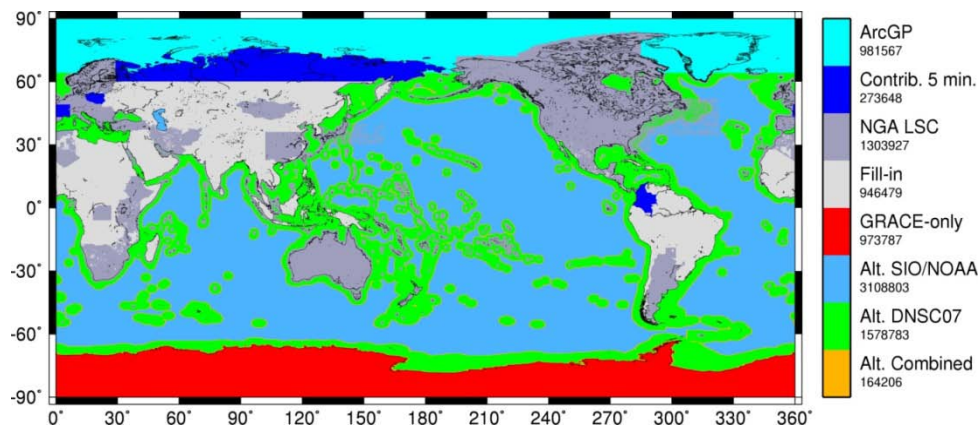

Fig. 1 Data sources for the EGM 2008 (*Pavlis et al.* 2008a, b, 2012)

Explanations:
"ArcGP": 5 x 5 minute mean gravity anomalies which were estimated as part of the Arctic Gravity Project.
"Contrib. 5 min": 5 x 5 minute mean gravity anomalies which were contributed to the project "ready-made". These mean values were estimated by the contributing person or agency.
"NGA LSC": 5 x 5 minute mean gravity anomalies which were estimated using Least Squares Collocation (LSC) by NGA.
"Fill-in": 5 x 5 minute mean gravity anomalies which were computed from the spectral "cut-and-paste" set of coefficients, where, up to $l = 720$ the coefficients represent the (proprietary) 5 x 5 minute mean gravity anomalies, and from $l=721$ to $L_{max} = 2159$ they represent the gravity anomalies implied by the Residual Terrain Model effects.
"Alt. SIO/NOAA": 5 x 5 minute mean gravity anomalies which were estimated by D. Sandwell and W. Smith, using altimetry data.
"Alt. DNSC07": 5 x 5 minute mean gravity anomalies which were estimated by O. Andersen and P. Knudsen, using altimetry data.
"Alt. Comb.": 5 x 5 minute mean gravity anomalies which were estimated as a linear combination of the SIO/NOAA and DNSC07 values (to avoid jump discontinuities).

The accuracy and resolution of the derivatives of the EGM 2008 geopotential for some of the mountain belts and other regions with the fill-in data can be several times lower than for the best covered areas. The fundamental question is what impact of this decrease on our computation results and their interpretations can be expected. Let us denote S (for signal) as the

magnitude of gravity anomalies in the selected point (area) on the Earth and N (for noise) as the relevant commission error (expressed in Fig. 2) for this area. More important than S and N alone is their ratio $\rho = S/N$ which should be (as is usual in statistics) $\gg 3$. Two different regions can be considered: the Central Europe with very precise gravity data, max $|S| = 150$ mGal and $N = 2$ mGal, and the Himalaya, max $|S| = 800$, $N\sim20$–40. The ratios ρ are 75 and 20-40, respectively, and there should not be any serious problem in the interpretation. However, ρ is valid for the gravity anomalies only and can be worse (smaller) for the other (higher) derivatives. For example, we do not have any commission error estimate available for the second radial derivative to assess the relevant ρ. The ratio also depends on the definition (on ranges of latitudes and longitudes) what it is "Central Europe" or "Himalaya" or another area.

In this paper, the formulae actually used for the first and second derivatives are not those of Hotine [15], but normalized equations summarized for T_i and Γ_{ij} ($i = x, y, z$; $ij = xx, yy, zz, xy, yz, xz$) as published in [26]. Eqs. (3)-(7) for the other aspects combine the second derivatives and were added into the computer program. The older foreign program [27], utilized intensively before 2009, limited in quantities computed from a gravity model, has been replaced by our own software [26].

In our figures, we make use of strongly non-linear scales to emphasize various features which otherwise might remain hidden. A note about the units of plotted functionals: milliGal [mGal] for the gravity anomalies and/or disturbances, E = Eötvös for the second order potential derivatives. The invariants I_1 and I_2 have units $[s^{-4}]$ and $[s^{-6}]$ and the ratio I is spaceless. The strike angle θ_S is expressed in degrees and its demonstration in red means its direction to the East and in blue to the West of the meridian. These units are used in all presented figures.

III. ASPECTS OF EGM 2008 IN VARIED REGIONS OF THE EARTH

A systematic screening was performed of correlations between aspects of the geopotential, as represented by the EGM 2008, and large-scale landform patterns displaying varied subsurface geological structures as well as climate-morphogenetic processes. Results of the screening are represented by means of selected examples from regions of various planation surfaces, high mountain ranges, collision zones of oceanic and continental lithospheric plates, regional fault zones, volcanic chains and large impact craters. Selected regions with demonstration of aspects from EGM 2008 were as follows [13-15]: the Nepal Himalaya and its neighbouring regions, further significant collision zone between lithospheric plates around Europe and Asia, morphotectonic contact between the Bohemian Massif, Eastern Alps and the Western Carpathians in Central Europe, the *collision zone of East-Asian and West-Pacific* lithospheric plates, the *contact region of north-eastern Africa, south-western Asia and south-eastern Europe* and regions of large impact craters such as Vredefort, Chicxulub and Popigai. Here we select the two areas written above in italics. More examples are on www.asu.cas.cz/~jklokocn.
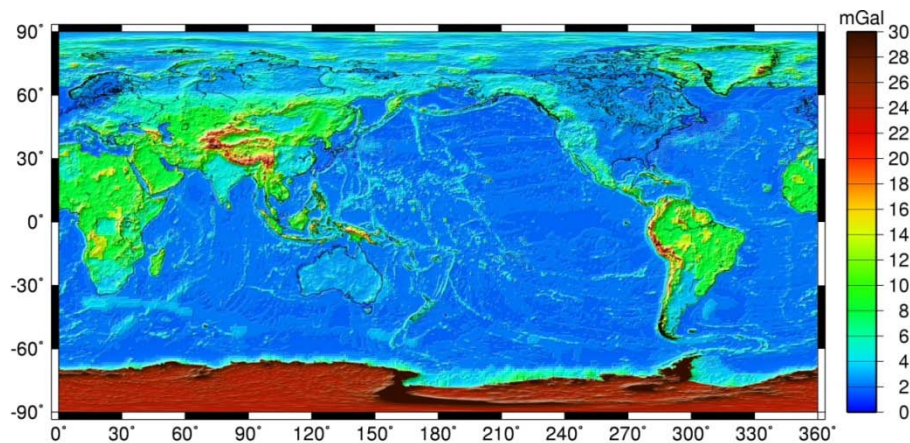

Fig. 2 Commission error (formal precision) of gravity anomalies 5 x 5 arcmin in EGM 2008, according to the authors of this gravity model: © Pavlis et al. [1]. Note large uncertainties over Antarctica (no terrestrial anomalies) and over some mountain belts (only the fill-in topography data available). Scale [milliGal]

By means of the evaluation of an extensive set of graphical representations of values of selected aspects of the geopotential (computed from the EGM 2008), it was found that the most effective information for diverse geo-applications is provided by (i) the radial second derivative of the disturbing gravitational potential Γ_{33} and (ii) the strike angle θ_S and 3) the virtual deformation of the ellipse of deformation. Variable values of Γ_{33} display significant gravitational signatures of extensive differences and changes in mass density and/or rock massif and regolith distributions. Local directions of strike angle θ_S form clusters, stripes and also zones with frequent space changes. These configurations of θ_S or of the virtual deformations can reflect and can be closely related to the directions of tectonic pressures in rock massifs of the near-surface part of the Earth's crust (e.g. [8]).

A. The Collision Zone of the East-Asian and West-Pacific Lithospheric Plates (Fig. 3)

The main large-scale patterns of the active collision zone between the Pacific (oceanic) and Asian (continental) plates are quite well expressed by the functionals Δg (Fig. 3a), Γ_{33} (Fig. 3d) and also partially by the ratio I (Fig. 3h) and strike angle θ_S

(Fig. 3i). Mountain chains of Japanese islands, including the huge massifs of stratovolcanoes, can be determined in Figs. 3 e,f,g, especially by the stripes and clusters of positive values of Δg and Γ_{33}. A striking feature drawn in Figs. 3 a,d,h,i is a remarkable arc of deep tectonic trenches connected with the active subduction of the Western-Pacific oceanic plate under the eastern margin of the Asian continental plate.

Virtual deformations derived from the ellipse of deformation (Fig. 3j) follow the positions of elevations and depressions of land and submarine reliefs. Demonstrated patterns of these virtual deformations are very similar to the occurrence of gravity anomalies Δg (Fig. 3a). The topographical features of the Kuril Islands, the Japanese Islands and groups of submarine volcanic massifs in the western part of the Pacific Ocean are especially noticeable, as expressed by positive values of Δg and/or virtual dilatations (compare Figs. 3a and 3b), and the Kuril and Japanese trenches are indicated by negative values of Δg and/or virtual contractions of the ellipse of deformation.

Fig. 3 (series). The Japanese Islands in the wide collision zone of the East-Asian and West-Pacific lithospheric plates.

3a
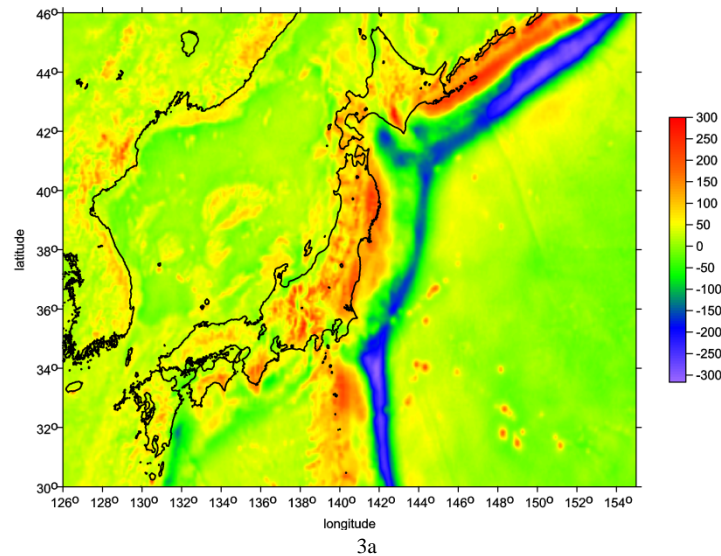
Fig. 3a Δg
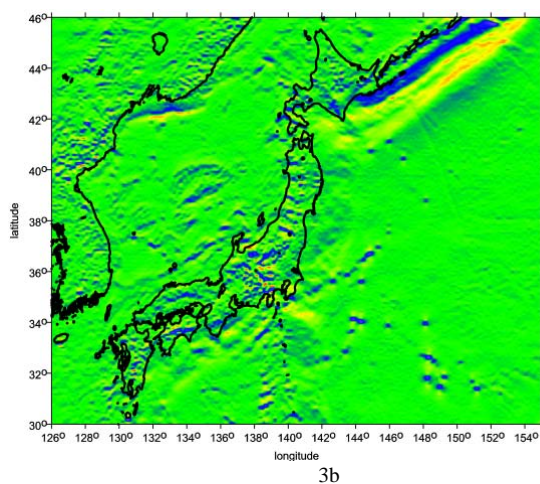
3b
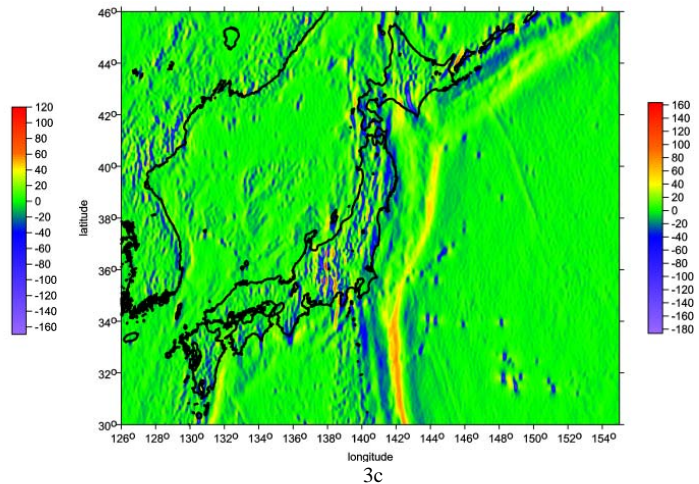
3c

Figs. 3b, 3c, 3d $\Gamma_{11}, \Gamma_{22}, \Gamma_{33}$
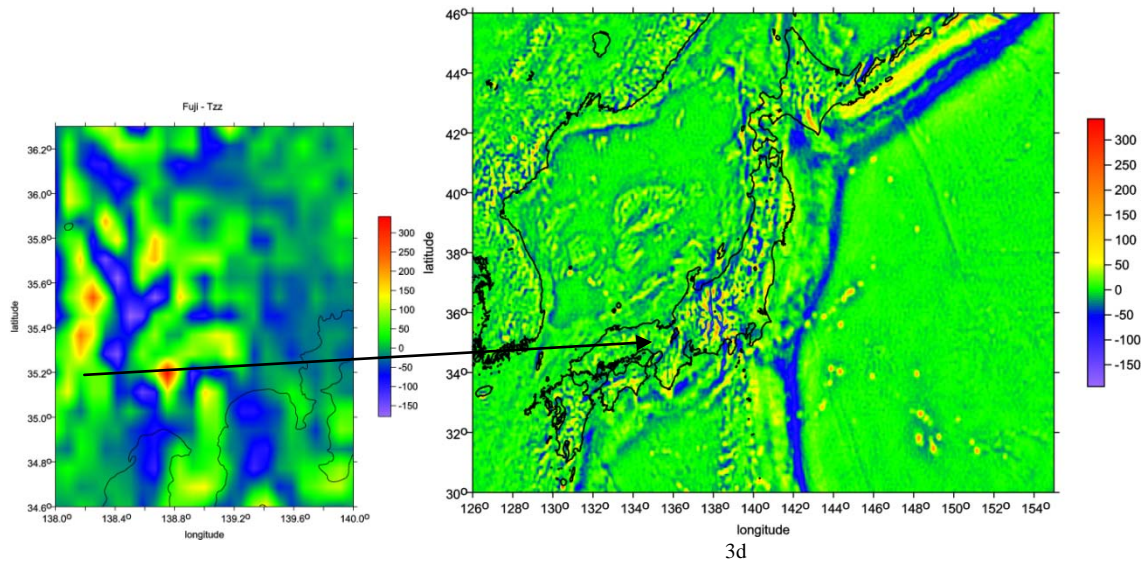
Fig. 3e Zoom for the Fuji area, Japan
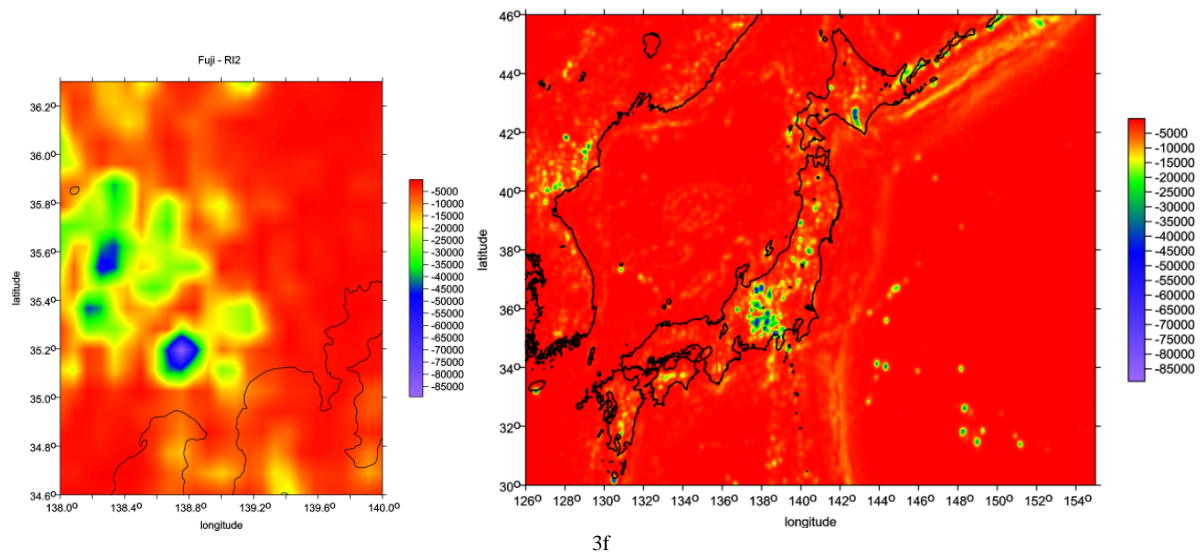
Fig. 3f I_1 for the area (right) with a zoom for the Fuji area (left)
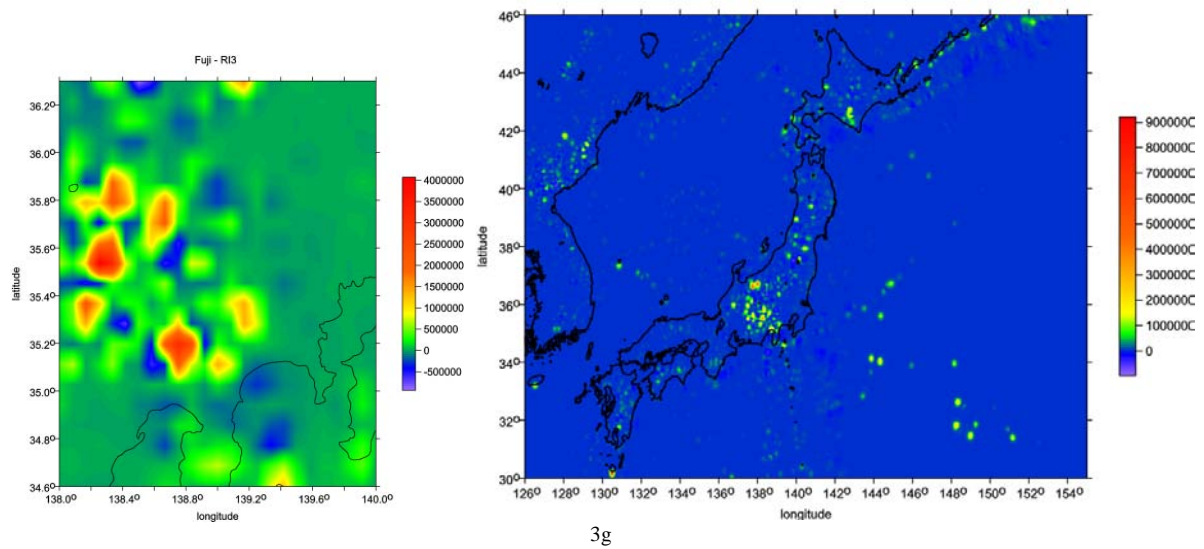
Fig. 3g I_2, with a zoom for the Fuji area (as above)

3h
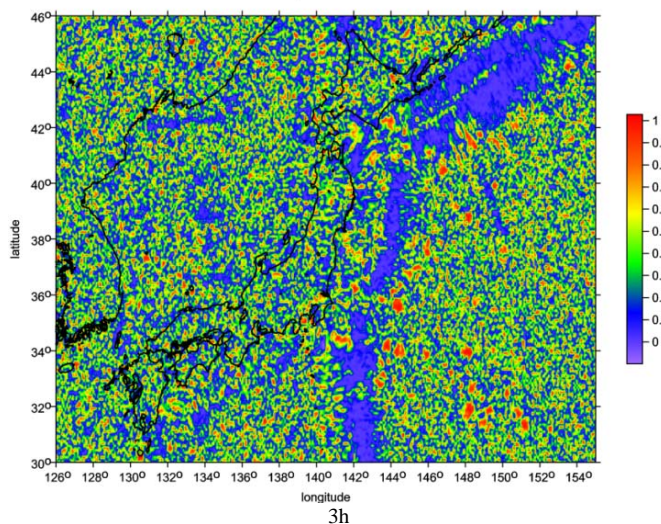
Fig. 3h The ratio *I*

3i
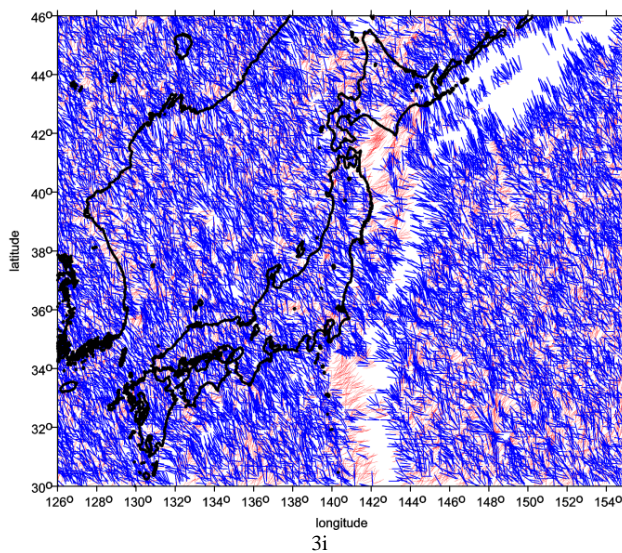
Fig. 3i The strike angle θ_S for the ratio $I > 0.3$


3j
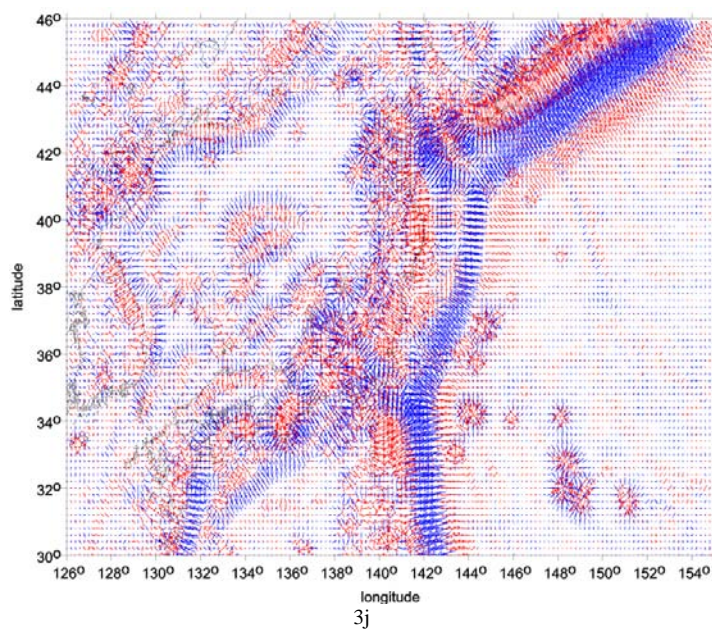
Fig. 3j The virtual deformations in the Pacific ocean and Japan, red - dilatation, blue - compression

B. Contact Region of North-Eastern Africa, South-Western Asia and South-Eastern Europe (Fig. 4)

The complicated geological structure and orographical patterns of the large contact region between these continents can be estimated especially from configurations of highly positive or negative values of Δg (Fig. 4a), Γ_{33} (Fig. 4d) and the strike angle θ_S (Fig. 4g). However, in comparison with the orogenetically very active Himalayan and West-Pacific areas, a presented scale of computed aspects of the EGM 2008 for this region suggests minor possibilities for geo-application. The main orographical patterns including the mountain ranges between the Balkans and the Iranian Highland as well as tectonic basins (e.g., in the Mediterranean Sea west of Cyprus and between Crete and the northern coast of Africa) are conspicuously expressed by Δg (Fig. 4a) and virtual deformations of the ellipse of deformation (Fig. 4h). Also remarkable are zones with significantly high positive values of Γ_{33} (Fig. 4d) combined with high negative values in close neighbourhoods. It is especially well rendered in regions of the Caucasus and Elborz Mountains as well as the narrow tectonic suture with the Dead Sea.

Fig. 4 (series). The broad contact region of north-eastern Africa, south-western Asia and south-eastern Europe, and a zoom for the Dead Sea area.


Fig. 4a Δg

4b

4c

Turkey - EGM08 - Tzz

4d
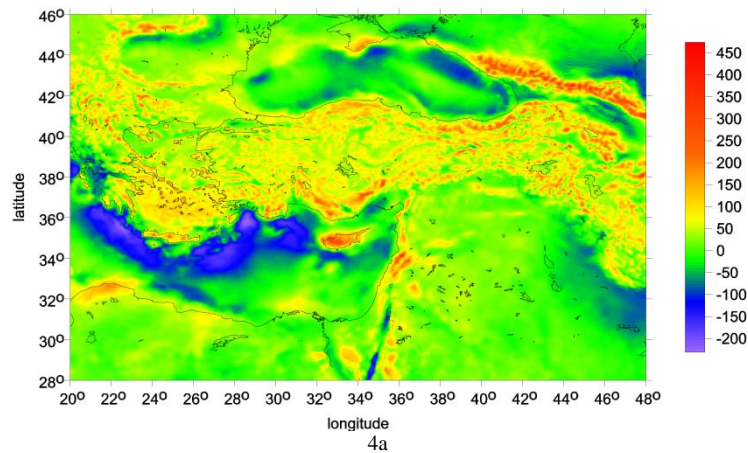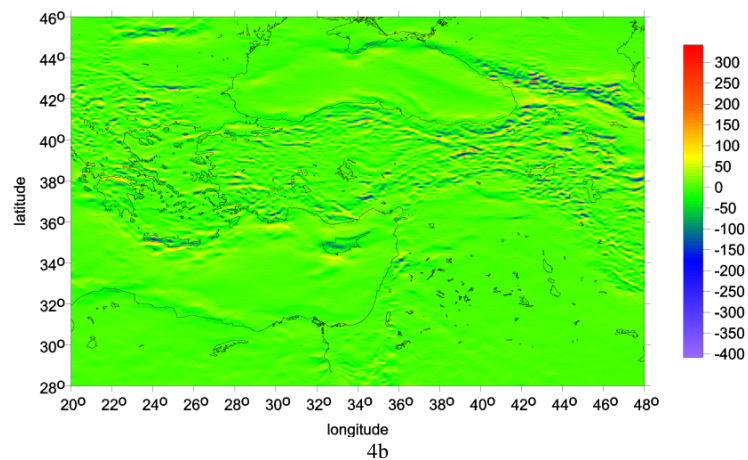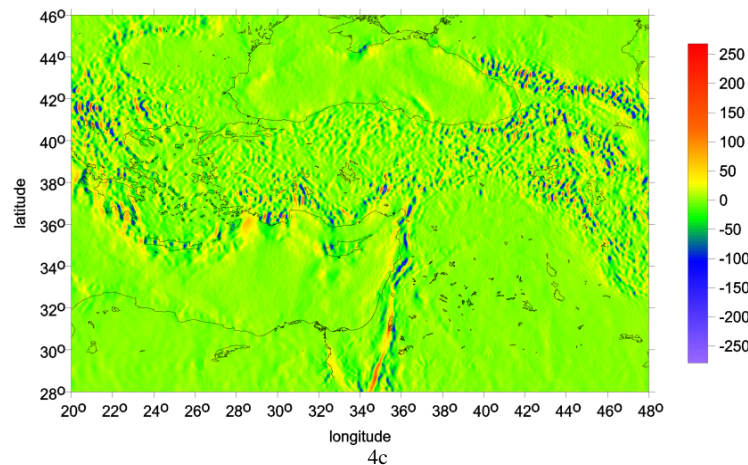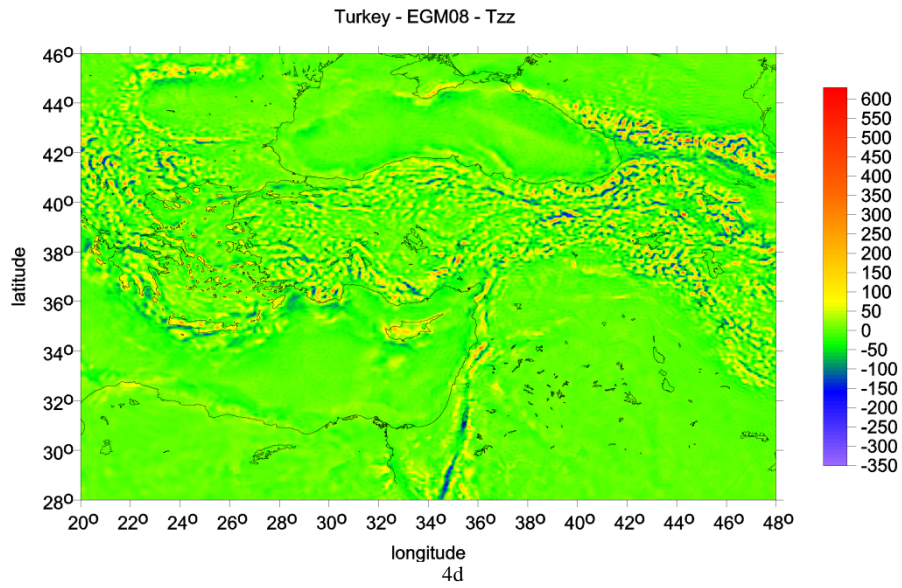
Figs. 4 b, 4c, 4d $\Gamma_{11}, \Gamma_{22}, \Gamma_{33}$


4e

Fig. 4e I_1

4f
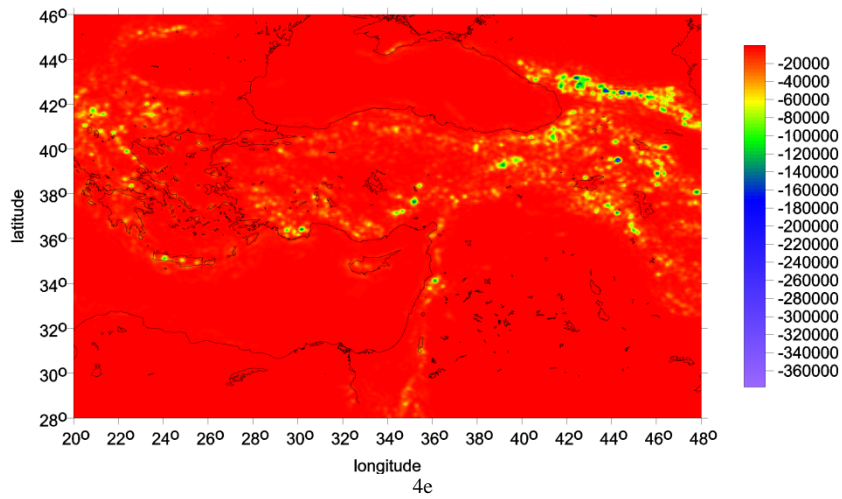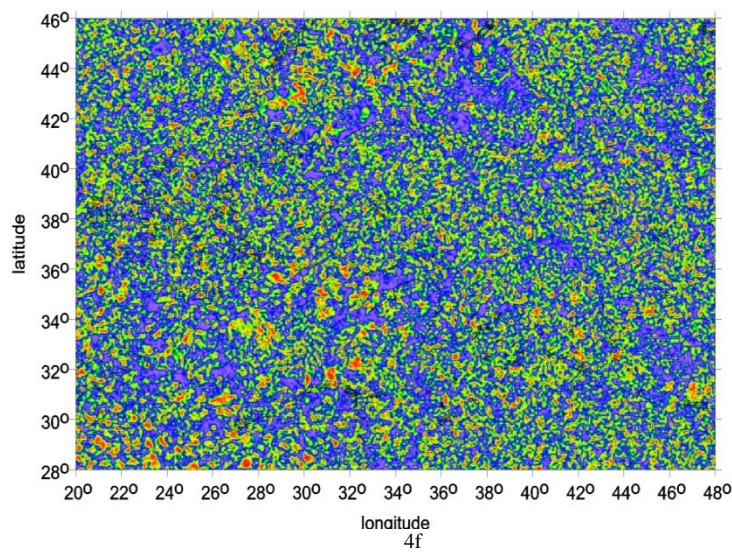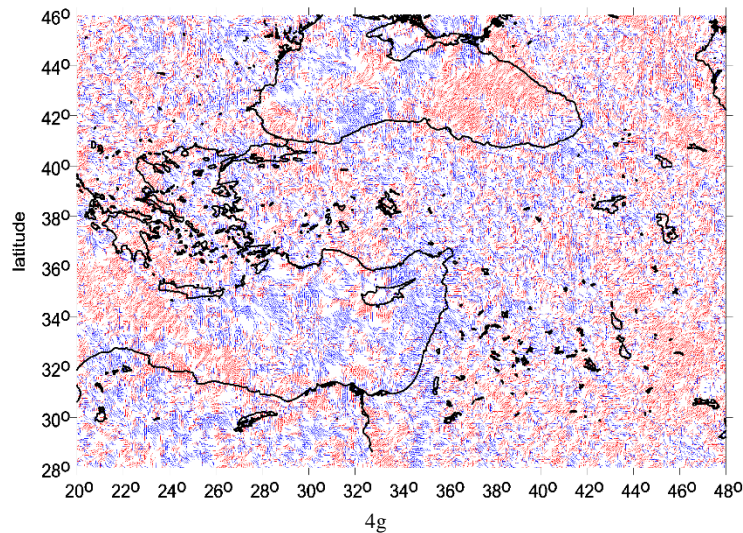
Fig. 4f The ratio I

Fig. 4g The strike angle θ_S for the ratio $I<0.3$
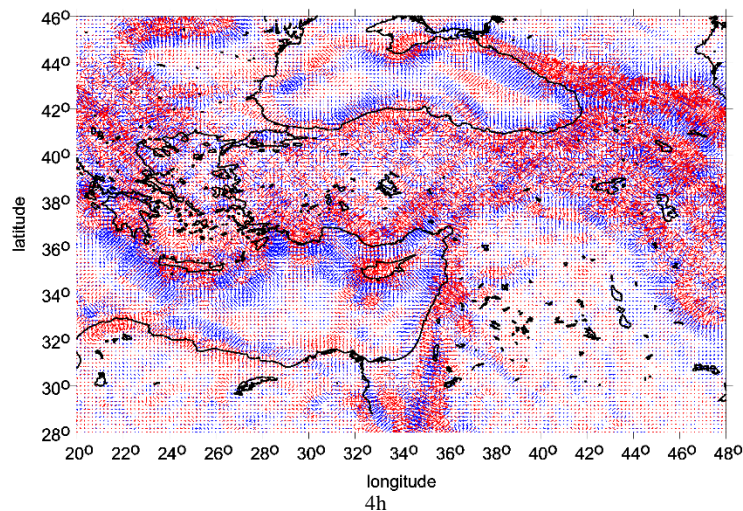

Fig. 4h The virtual deformations

Figs. 4i, 4j, 4k, 4l demonstrate selected details for the Dead Sea region (including part of the Easternmost Mediterranean, territory of Israel and part of Jordan territory). It is presented as one of key regions in which a comparison of our results derived from the EGM 2008 with the well-known geophysical features and geological situation can be documented. This region contains several tectonic units: Judea-Samaria, Galilee-Lebanon, Antilebanon, Negev, Heletz and Pleshet Basin (Eppelbaum and Katz [28]).

Geological-geophysical analysis of satellite derived gravity field (Fig. 4i) and its aspects (Figs. 4j, 4k and 4l) allow to make the following conclusions:

(1) Dead Sea Transform (DST), where strong negative gravity anomalies are caused by thick accumulation of series of low-density sedimentary deposits and salts, is clearly detected in Figs. 4i and 4k (here only part of the developed maps is shown). The linear compression zone along the DST is displayed by the virtual deformations (Fig. 4l, also Fig. 4h).

(2) The area of Makhtesh Ramon Canyon is characterized by uplift of deep geological associations of heightened density (Fig. 4i).

(3) A source of Carmel gravity anomaly is uplift of crystalline basement (Fig. 4i).

(4) Hebron gravity anomaly is probably produced by the high-dense mantle diapir (Figs. 4i, 4k).

(5) Basalt plateau in Jordan is reflected by positive anomalies (it is caused by significant difference between density of basalts and surrounding sedimentary deposits) - (Figs. 4i, 4k).

(6) To east of the Dead Sea, some of gravity anomalies may be caused by known uplift of the crystallic basement (Figs. 4i and 4k), [8].

(7) The map of the strike angles (Fig. 4j) enables to recognize a dominant location of some subsurface masses and shows very complex distribution of the studied parameters.


4i
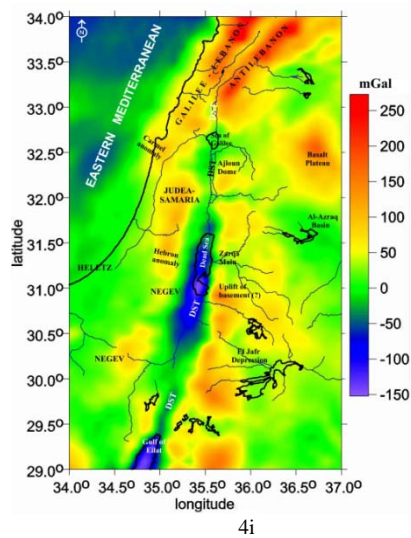
Fig. 4i Δ*g* (The Dead Sea region)

4j
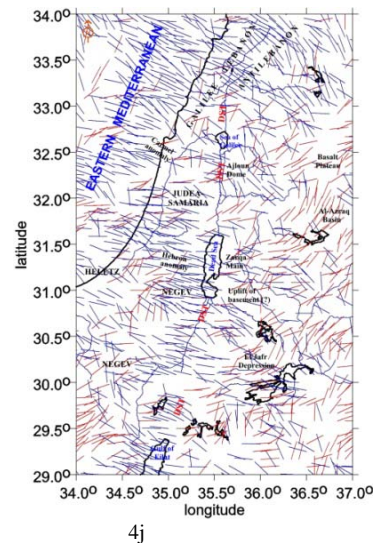
Fig. 4j The Dead Sea, zoom: The strike angle θ_S for $I<0.3$



4k
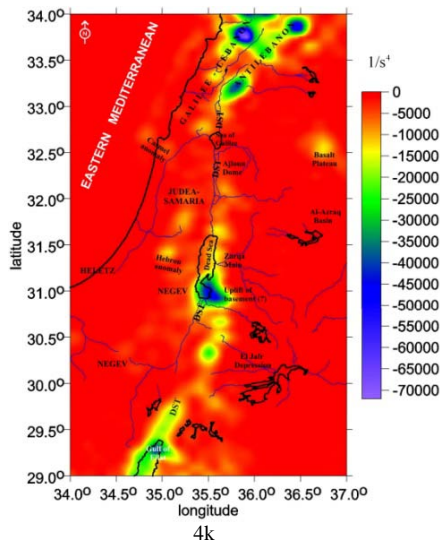
Fig. 4k I_1 (The Dead Sea)

4l
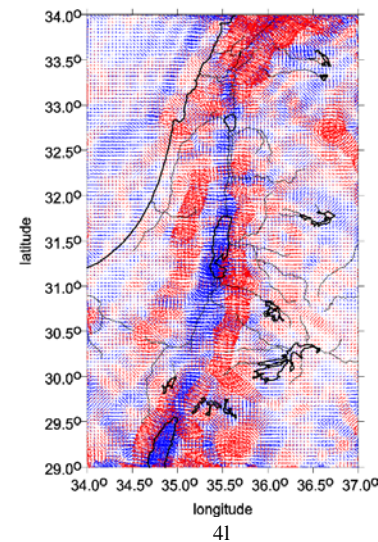
Fig. 4l The Dead Sea: the virtual deformations

IV. DISCUSSION

The presented examples of the geomorphic and geological aspects of the EGM 2008 in geodynamically varied regions of the Earth enable to underline some general findings and related remarks. The long-term activity of climate-morphogenetic processes in tectonically calm regions and in areas of active epeirogenesis resulted in the development of large planation surfaces and lowlands which are very close to geophysical levels of the same gravitational potential. Therefore, it was found that on large-scale planation surfaces and topographically similar landforms, smoothed by denudation or accumulation of different genesis and age, values of the second derivatives of the disturbing gravitational potential Γ_{33} are only in the range of approximately ±100 Eötvös [14, 15]. On the contrary, regions of active orogeny and related morphotectonic processes are characterized by conspicuous compressions of rock massifs in the near-surface part of the Earth's crust and a very variable topographic mass distribution. These landform patterns are displayed by significantly high positive and/or negative values of Γ_{33}. High negative values of Γ_{33} have been indicated in regions of tectonically conditioned discontinuities or sinking of the Earth's surface and in regions with very intense erosion of rocks and transport of regolith.

It is probable that similar opinion can be expressed as an explanation of striking anomalies of the invariants. In regions with very noticeable features of active morphotectonic and erosion processes, very significant negative values I_1 and, on the contrary, positive values of I_2 were identified. Similarly, it is possible to express and verify the hypothesis that directions of strike angle θ_S to a certain degree represent, or are in a harmony with, the prevailing directions of tectonic pressures and

tensions in the near-surface part of the Earth's crust. Significant coincidences are also detected between regional patterns of Γ_{33} and virtual deformations of the ellipse of deformation.

V. CONCLUSIONS

The existing theory of Pedersen and Rasmussen [7] and Beiki and Pedersen [8] has been extended here. It was applied in various regions of the Earth, using the global gravitational field model EGM 2008 with a resolution of ~10 km on the Earth's surface. For the first time a global or regional view is on offer - that is not only local as till now, based on airborne gradiometry or classical gravimetric data. Aims of this paper consisted in presentation of methodological principles and expression of computed gravity features (the aspects) in selected regions of the Earth (few examples), not in deep interpretations.

Comparison of the displayed results of aspects of the geopotential, computed by the EGM 2008 on a sub-continental scale with their details in smaller regions [12-15] confirms the very perspective possibilities and advantages of an integrated approach to various applications in the Earth sciences. Records of the present state of quantitative characteristics of the near-surface part of the geoid also make it possible to assess the recent dynamics of landform processes.

Correlations of large-scale landform configurations with some aspects of the EGM 2008, particularly the radial second derivatives of the disturbing gravitational potential Γ_{33}, the strike angle θ_S and virtual deformations, are demonstrated in the selected regions of the Earth. It is suggested that landform patterns with very conspicuous combinations of significantly high positive or negative values of Γ_{33} are under the strong influence of rapid and/or intensive geomorphic processes. Strong coincidences between a large-scale landform configuration of selected regions and the extension of areas with very high positive values of the radial second derivative of the disturbing gravitational potential Γ_{33}, and the most likely in combination with conspicuous areas of high negative values of Γ_{33} in their close neighbor have been identified. These geophysical signatures, supported by values of the strike angle θ_S and virtual dilatations or compressions, reflect the regional dynamics of Earth's surface evolution.

ACKNOWLEDGMENTS

REFERENCES

[1] N. K. Pavlis, S. A. Holmes, S. C. Kenyon, and J.K. Factor, "EGM2008: An overview of its development and evaluation," National Geospatial-Intelligence Agency, USA, conf.: Gravity, Geoid and Earth Observation 2008, Chania, Crete, Greece, 23-27 June, 2008.

[2] N. K. Pavlis, S. A. Holmes, S. C. Kenyon, and J. K. Factor, "An Earth Gravitational Model to degree 2160: EGM 2008," EGU General Assembly 2008, Vienna, 13-18 April 2008.

[3] N. K. Pavlis, S. A. Holmes, S. C. Kenyon, and J. K. Factor, "The development and evaluation of the Earth Gravitational Model 2008 (EGM2008)," J. Geophys., Res. 17, B04406, DOI: 10.1029/2011JB008916, 2012.

[4] T. Mayer-Guerr, "ITG-Grace03s: The latest GRACE gravity field solution computed in Bonn," presentation at GSTM+SPP symp., Potsdam, 15-17 Oct. 2007.

[5] J. Kalvoda, J. Klokočník, J. Kostelecký, and A. Bezděk, "Mass distribution of Earth landforms determined by aspects of the geopotential as computed from the global gravity field model EGM 2008," Acta Univ. Carolinae, Geographica, XLVIII, 2, Prague, 2013.

[6] R. Floberghagen, M. Fehringer, D. Lamarre, D. Muzi, B. Frommknecht, Ch. Steiger, J. Pineiro, and A. da Costa, "Mission design, operation and exploitation of the gravity Field and steady-state ocean circulation explorer mission," J. Geod., vol. 85, pp. 749-758; http://dx.doi.org/10.1007/s00190-012-0541-z, 2011.

[7] B. D. Pedersen and T. M. Rasmussen, "The gradient tensor of potential field anomalies: Some implications on data collection and data processing of maps," Geophysics, vol. 55, pp. 1558-1566, 1990.

[8] M. Beiki and L. B. Pedersen, "Eigenvector analysis of gravity gradient tensor to locate geologic bodies," Geophysics, vol. 75, pp. 137-149, DOI: 10.1190/1.3484098, 2010.

[9] J. Mataragio and J. Kieley, "Application of full tensor gradient invariants in detection of intrusion-hosted sulphide mineralization: Implications for deposition mechanisms," Mining Geoscience, EAGE First Break, vol. 27, pp. 95-98, 2009.

[10] C. A. Murphy and J. L. Dickinson, "Exploring exploration play models with FTG gravity data," 11th SAGA Biennal Techn. Meeting & Exhib., Swaziland, pp. 89-91, 16-18 Sept. 2009.

[11] A. H. Saad, "Understanding gravity gradients - a tutorial, the meter reader," ed. B. Van Nieuwenhuise, August issue, The Leading Edge, pp. 941-949, 2006.

[12] J. Klokočník (ed.), "Detection of Hidden Impact (Meteoritic) Structures: Introduction to study and simulations before the GOCE launch," report: Grant ESA/PECS C-98056: "GOCE - Specific tasks on fine gravity field structure of the Earth," Report of Astronom. Inst. Czech Acad. Sci., Ondřejov Obs., p. 101, 2008.

[13] J. Klokočník, J. Kostelecký, I. Pešek, P. Novák, C. A. Wagner, and J. Sebera, "Candidates for multiple impact craters? Popigai and Chicxulub as seen by the global high resolution Gravitational Field Model EGM08," Solid Earth EGU 1, pp. 71-83, DOI: 10.5194/se-1-71-2010, 2010.

[14] J. Kalvoda, J. Klokočník, and J. Kostelecký, "Regional correlation of the Earth Gravitational Model 2008 with morphogenetic patterns of the Nepal Himalaya," Acta Univ. Carolinae, Geographica, XLV, vol. 2, pp. 53-78, Prague, 2010.

[15] M. Hotine, "Mathematical Geodesy," ESSA, US. Dept. Comm., Environ. Sci. Serv. Admin., Monograph 2, Washington D.C., 1969.

[16] G. Balmino, "Proposition pour les arcs GRADIO, Gradiométrie par satellite," Special report of CNES 1981, Toulouse.

[17] R. Rummel and O. L. Colombo, "Gravity field determination from satellite gradiometry", Bull. Geod., vol. 59, pp. 233-246, 1985.

[18] R. Rummel, "Satellite gradiometry - A promising concept for 25 years," Verlag der Bayerischen Akademie der Wissenschaften, vol. 48, pp. 122-139, München, 1986.

[19] R. Rummel, "Satellite gradiometry," in: H. Sünkel (ed.), Mathematical and Numerical Techniques in Physical Geodesy, Lecture Notes in Earth Sciences, vol. 7, pp. 317-363, Springer, ISBN (Print) 978-3-540-16809-6, DOI: 10.1007/BFb0010135, 1986.

[20] A. Marussi, "Microgravitation in space," Geophysical Journal of the Royal Astronomical Society, vol. 76, pp. 691–695, DOI: 10.1111/j.1365-246X.1984.tb01917.x, 1984.

[21] O. Baur, N. Sneeuw, and E. Grafarend, "Methodology and use of tensor invariants in satellite gravity gradiometry", J. Geod., vol. 82, pp. 279–293, 2008.

[22] P. Holota, "Boundary value problems and invariants of the gravitational tensor in satelite gradiometry", Lecture Notes in Earth Science, vol. 25, Springer, pp. 447-457, 1989.

[23] B. Pawlowski, "Gravity gradiometry in resource exploration," The Leading Edge, vol. 17, pp. 51-52, 1998.

[24] X. Li, "Vertical resolution: Gravity versus vertical gravity gradient," The Leading Edge, vol. 20, pp. 901-904, 2001.

[25] M. Brdička, L. Samek, and B. Sopko, "Mechanika kontinua," (Continuum Mechanics), Academia Praha, 2000(in Czech).

[26] J. Sebera, C. A. Wagner, A. Bezděk, and J. Klokočník, "Short guide to direct gravitational field modelling with Hotine's equations," J. Geod., vol. 87, pp. 223-238. [Online]. Available: http://dx.doi.org/10.1007/s00190-012-0591-2, 2013.

[27] S. A. Holmes, N. K. Pavlis, and P. Novák, "A Fortran program for very-high degree harmonic synthesis," version 05/01/2006.

[28] L. V. Eppelbaum and Y. I. Katz, "Tectonic-Geophysical mapping of Israel and Eastern Mediterranean: Implication for hydrocarbon prospecting," Positioning, vol. 2, pp. 36-54, 2011.